

# Modeling of asymmetrical boost converters

## Modelado de convertidores, elevadores asimétricos

E. I. Arango Zuluaga<sup>1</sup>, C. A. Ramos-Paja<sup>2</sup> and A. J. Saavedra-Montes<sup>3</sup>

### ABSTRACT

The asymmetrical interleaved dual boost (AIDB) is a fifth-order DC/DC converter designed to interface photovoltaic (PV) panels. The AIDB produces small current harmonics to the PV panels, reducing the power losses caused by the converter operation. Moreover, the AIDB provides a large voltage conversion ratio, which is required to step-up the PV voltage to the large dc-link voltage used in grid-connected inverters. To reject irradiance and load disturbances, the AIDB must be operated in a closed-loop and a dynamic model is required. Given that the AIDB converter operates in Discontinuous Conduction Mode (DCM), classical modeling approaches based on Continuous Conduction Mode (CCM) are not valid. Moreover, classical DCM modeling techniques are not suitable for the AIDB converter. Therefore, this paper develops a novel mathematical model for the AIDB converter, which is suitable for control-purposes. The proposed model is based on the calculation of a diode current that is typically disregarded. Moreover, because the traditional correction to the second duty cycle reported in literature is not effective, a new equation is designed. The model accuracy is contrasted with circuital simulations in time and frequency domains, obtaining satisfactory results. Finally, the usefulness of the model in control applications is illustrated with an application example.

**Keywords:** DC/DC switching converters, asymmetrical interleaved, modeling, discontinuous conduction mode.

### RESUMEN

El conversor elevador, asimétrico y entrelazado (AIDB) es un conversor CD/CD de quinto orden, diseñado para las aplicaciones fotovoltaicas (PV). El AIDB produce armónicos de corriente bajos a los paneles PV, reduciendo así, la pérdida de potencia causada por la operación del conversor. Además, el AIDB provee un alto factor de transformación del voltaje requerido en enlaces de CD y utilizado en los inversores conectados a la red. Pero para rechazar perturbaciones ambientales o de carga, se requiere operar el AIDB en lazo cerrado, y por lo tanto, es necesario disponer de un modelo dinámico.

En tal ámbito, las técnicas clásicas de modelado en modo continuo (CCM) no son válidas, debido a que el AIDB opera en modo discontinuo (DCM) y las técnicas clásicas de control en DCM no son aplicables al AIDB. De esta manera, el presente artículo propone una nueva aproximación de modelado para el AIDB, orientada al control; el modelo propuesto se basa en el cálculo de la corriente de un diodo, típicamente no tenida en cuenta. Asimismo, debido a que la corrección del segundo ciclo de trabajo reportada en la literatura no es aplicable al AIDB, este artículo presenta una nueva ecuación. El modelo se valida a través de una comparación, en los dominios de tiempo y frecuencia, con simulaciones circuitales. Finalmente, se muestra la utilidad del modelo en las aplicaciones de control mediante un ejemplo práctico.

**Palabras clave:** conversores CD/CD, entrelazado asimétrico, modelado, modo de conducción discontinuo.

Received: December 12th 2012

Accepted: November 14th 2013

### Introduction

Solar powered systems are efficient alternatives for providing redundancy for critical applications, in situ energy generation and reducing production of traditional energy that impacts the environment, for both portable and residential applications (Ouyang, Cheng, Zhang and Yao, 2010).

In particular, photovoltaic (PV) generation systems require power converters to adjust the PV panels' operating point to maximize

the power production (Veerachary, Senjyu and Uezato, 2001). Such a power conversion system has been designed adopting single stage inverters (Jain and Agarwal, 2007) or adopting double stage structures based on DC/DC and DC/AC converters (Ilango and Rajasekar, 2009). Yet, due to the possibility of performing, both the tracking of the maximum power point (MPPT) and power factor correction in the connection with the grid (Ilango and Rajasekar, 2009), the double stage solutions are widely accepted in

<sup>1</sup> Eliana Isabel Arango Zuluaga. Ingeniera Electrónica, Universidad de Antioquia, Colombia. Doctora en Ingeniería Electrónica, Universitat Rovira i Virgili, España. Affiliation: Profesora Asistente, Universidad Nacional de Colombia, Colombia. E-mail: eiarangoz@unal.edu.co

<sup>2</sup> Carlos Andrés Ramos-Paja. Ingeniero Electrónico y Magister en Automática, Universidad del Valle, Colombia. Master en Ingeniería Electrónica y Doctor en Electrónica de Potencia, Universitat Rovira i Virgili, España. Affiliation: Profesor Asociado, Universidad Nacional de Colombia, Colombia. E-mail: caramosp@unal.edu.co

<sup>3</sup> Andrés Julián Saavedra-Montes. Ingeniero Electricista, Universidad del Valle, Colombia. Magister en Sistemas de Generación de Energía Eléctrica y Doctor en Ingeniería, Universidad del Valle, Colombia. Affiliation: Profesor Asociado, Universidad Nacional de Colombia, Colombia. E-mail: ajsaaved@unal.edu.co

**How to cite:** Arango, E. I., Ramos-Paja, C. A., Saavedra-Montes, A. J., Modeling of asymmetrical boost converters., Ingeniería e Investigación, Vol. 34, No. 1, April, 2014, pp. 53 – 59.

distributed generation systems (Ahmed, Miyatake, and Al-Othman, 2008), stand-alone DC applications (Arango, Ramos-Paja and Saavedra-Montes, 2012) and hybrid power systems (Ilango and Rajasekar, 2009; Ahmed et al., 2008).

Since the PV panels provide low voltages (Veerachary et al., 2001; Arango et al., 2012), and taking into account that grid-connected inverters require large input voltages (Arango et al., 2012), the DC/DC converter most commonly used for the first stage of such systems is the classical boost converter (Ahmed et al., 2008). Moreover, such a topology demands a continuous current from the PV panel, which avoids oscillations around the Maximum Power Point (MPP) that reduce the generated power.

In the boost converter, the current ripples injected into the PV generators depend on the inductor size, switching frequency, input capacitor and power source high frequency impedance. This has been addressed by using interleaving structures (Giral, Martinez-Salamero and Singer, 1999), which considers the connection of parallel DC/DC converters to share the power flow between two or more branches. Such a technique has been successfully adopted in photovoltaic applications (Veerachary et al., 2001), but traditional interleaving structures require current control loops in each phase to ensure a proper current sharing among the parallelized converters, which increases the control complexity.

To provide the high voltage conversion ratio and low current ripples required in PV applications, an interleaved structure based on boost converters and voltage multiplier cells (VMC) (Prudente, Pfitscher, Emmendoerfer, Romaneli, and Gules, 2008) was proposed in (Arango et al., 2012). This structure is the asymmetrical interleaved dual boost converter (AIDB) and is depicted in Fig. 1. The AIDB converter was derived by breaking the symmetry of two interleaved boost converters connected in parallel with a VMC. A detailed description of such a procedure is given in (Arango et al., 2012).

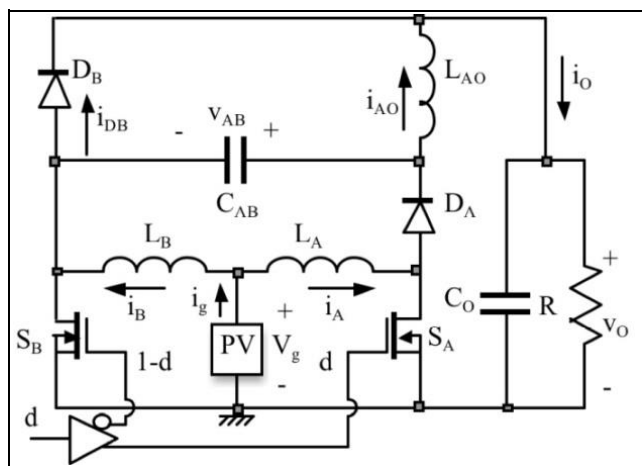


Figure 1. AIDB DC/DC converter

The AIDB provides a higher conversion ratio in comparison to the traditional interleaved boost converter, but preserving the small input current and output voltage ripples characteristic. In addition, the AIDB does not require internal current control loops to ensure the current sharing among the parallelized converters due to its inherent operation on Discontinuous Conduction Mode (DCM). Moreover, the AIDB exhibits an additional feature: the voltage conversion ratio and steady-state currents do not depend on the load impedance, despite its operation on DCM, which is not the case with traditional converters (Erickson and Maksimovic, 2001). Therefore, taking into account that PV systems operate in

non-constant load conditions, the AIDB is simpler to design than classical solutions, in which the steady-state behavior depends on the circuit parameters and load impedance.

The previous characteristics make the AIDB converter an excellent option to design PV systems. Yet, in order to reject disturbances present in grid-connected PV systems, or in any application of the AIDB, the DC/DC converter must be operated in a closed loop (Jain and Agarwal, 2007). To design such control systems a dynamic small-signal model is required. However, as anticipated before, the AIDB converter always operates in DCM, therefore the classical modeling approach in Continuous Conduction Mode (CCM) is not suitable for the AIDB (Arango et al., 2012). To model DCM converters, the approach given by Sun, Mitchell, Greuel, Krein, and Bass (2001) is commonly adopted, which provides a methodology to correct the prediction of the discontinuous interval. Nevertheless, the solution described by Sun et al. (2001) is not applicable to the AIDB converter, since such a method produces a mathematical cancelation of some state variables, producing a large error. Such a condition is illustrated in Section 3.

This paper proposes a new modeling approach designed for the AIDB converter, which has the main objective of providing a control-oriented small-signal model. The novel modeling approach is based on the circuit analysis of the AIDB converter presented in Section 2, and uses the new method to correct the discontinuous interval prediction presented in Section 4. Then, the proposed AIDB model, summarized in Section 5, is validated by contrasting its performance with the circuit simulation of the non-linear circuit in Section 6.

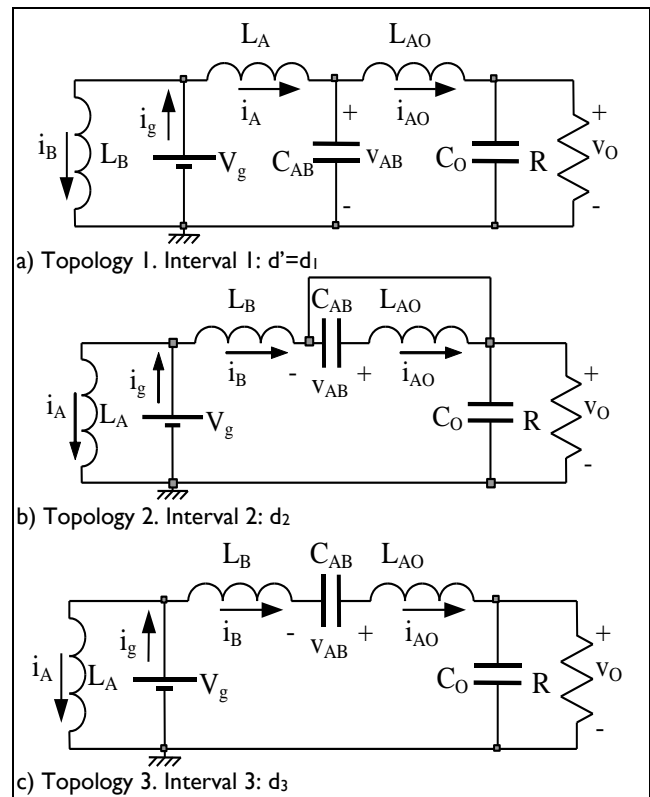


Figure 2. AIDB topologies

### AIDB topologies and equations

The AIDB converter, depicted in Fig. 1, is basically a parallel interconnection between a boost converter with an output filter

(branch A) and a traditional boost converter (branch B) in which the first capacitor of the A-branch output filter is connected to the intermediate node of the boost of the B-branch. This method follows the concept of switching capacitor-based voltage multiplier cells. The MOSFETs  $S_A$  and  $S_B$  are activated in a complementary way to obtain the input current ripple reduction.

The AIDB topologies, the sequence of operation and the interval duration have all been analyzed in detail in (Arango et al., 2012), where the duty cycle  $D$  must be constrained to  $D > 0.382$  to ensure the correct behavior. Fig. 2 shows the AIDB topologies obtained by means of the classical approach given in (Erickson and Maksimovic, 2001):

- Topology 1:  $S_B$  and  $D_A$  ON;  $S_A$  and  $D_B$  OFF. Interval 1:  $d'=d_1$ .
- Topology 2:  $S_A$  and  $D_B$  ON;  $S_B$  and  $D_A$  OFF. Interval 2:  $d_2$ .
- Topology 3:  $S_A$  ON;  $S_B$ ,  $D_A$  and  $D_B$  OFF, where  $D_B$  is in DCM. Interval 3:  $d_3$ .

The operation sequence Topology 1-Topology 2-Topology 3 provides low input current and output voltage ripples, which are required for photovoltaic systems. Moreover, the operation intervals are related as follows:

$$d_1 + d_2 + d_3 = 1, d_1 = d', d_2 + d_3 = d \quad (1)$$

The differential equations in the first topology are:

$$\begin{aligned} L_A \frac{di_A}{dt} &= v_g - v_{AB}, L_B \frac{di_B}{dt} = v_g, L_{AO} \frac{di_{AO}}{dt} = v_{AB} - v_O \\ C_{AB} \frac{dv_{AB}}{dt} &= i_A - i_{AO}, C_O \frac{dv_O}{dt} = i_{AO} - \frac{v_O}{R} \end{aligned} \quad (2)$$

Similarly, for the second topology are the following:

$$\begin{aligned} L_A \frac{di_A}{dt} &= v_g, L_B \frac{di_B}{dt} = v_g - v_O, L_{AO} \frac{di_{AO}}{dt} = v_{AB} \\ C_{AB} \frac{dv_{AB}}{dt} &= -i_{AO}, C_O \frac{dv_O}{dt} = i_B - \frac{v_O}{R} \end{aligned} \quad (3)$$

Finally, for the third topology they are the following:

$$\begin{aligned} L_A \frac{di_A}{dt} &= v_g, i_{AO} = i_B * \\ (L_B + L_{AO}) \frac{di_B}{dt} &= v_g + v_{AB} - v_O \\ C_{AB} \frac{dv_{AB}}{dt} &= -i_{AO}, C_O \frac{dv_O}{dt} = i_{AO} - \frac{v_O}{R} \end{aligned} \quad (4)$$

In the equations system of the third topology (4), the equation marked with an asterisk (\*) reflects the reduction of order that occurs in the discontinuous mode that makes it difficult to perform the averaging calculations in the state space. Such a condition will be evident in the next section.

## Revised averaging method

The revised averaging modeling method for DCM operation was introduced in Sun et al. (2001), and it consists of three steps: averaging, correction and duty-ratio constraint.

The averaging consists of adding the products of the topology equations and their corresponding intervals. The state space averaged system for the AIDB is:

$$\begin{aligned} \frac{d\bar{i}_A}{dt} &= \frac{v_g - \bar{v}_{AB} d_1}{L_A} \\ \frac{d\bar{i}_B}{dt} &= \frac{v_g}{L_B} (d_1 + d_2) - \frac{\bar{v}_O}{L_B} d_2 + \frac{v_g - \bar{v}_O + \bar{v}_{AB}}{L_B + L_{AO}} d_3 \\ \frac{d\bar{i}_{AO}}{dt} &= \frac{\bar{v}_{AB}}{L_{AO}} (d_1 + d_2) - \frac{\bar{v}_O}{L_{AO}} d_1 + \frac{v_g - \bar{v}_O + \bar{v}_{AB}}{L_B + L_{AO}} d_3 \\ \frac{d\bar{v}_{AB}}{dt} &= \frac{\bar{i}_A d_1 - \bar{i}_{AO}}{C_{AB}}, \frac{d\bar{v}_O}{dt} = \frac{\bar{i}_{AO}}{C_O} - \frac{\bar{v}_O}{RC_O} \end{aligned} \quad (5)$$

The correction consists in dividing all the inductor currents in the converter by the factor  $(d_1+d_2)$  because these are the two duty ratios in which the inductors are conducting. This correction must be made because in DCM the inductor currents have three intervals instead of the two intervals exhibited in CCM. Therefore, the classical CCM averaging procedure is not appropriate for DCM.

From the topology equations of the AIDB converter, it is noted that  $L_A$  current  $i_A$  has two intervals (second and third topologies have the same equation), while  $L_B$  and  $L_{AO}$  currents ( $i_B$  and  $i_{AO}$ , respectively) exhibit three intervals. Therefore, in order to model the AIDB converter it is only necessary to apply the correction to the equations concerning  $i_B$  and  $i_{AO}$  given that the averaging of  $i_A$  is already correct. Consequently, the right side of the averaging equations of  $i_B$  and  $i_{AO}$  are divided by the factor  $(d_1+d_2)$ , to obtain the following corrected averaging system:

$$\begin{aligned} \frac{d\bar{i}_A}{dt} &= \frac{v_g - \bar{v}_{AB} d_1}{L_A} \\ \frac{d\bar{i}_B}{dt} &= \frac{v_g}{L_B} + \frac{1}{d_1 + d_2} \left[ -\frac{\bar{v}_O}{L_B} d_2 + \frac{v_g - \bar{v}_O + \bar{v}_{AB}}{L_B + L_{AO}} d_3 \right] \\ \frac{d\bar{i}_{AO}}{dt} &= \frac{\bar{v}_{AB}}{L_{AO}} + \frac{1}{d_1 + d_2} \left[ -\frac{\bar{v}_O}{L_{AO}} d_1 + \frac{v_g - \bar{v}_O + \bar{v}_{AB}}{L_B + L_{AO}} d_3 \right] \\ \frac{d\bar{v}_{AB}}{dt} &= \frac{\bar{i}_A d_1 - \bar{i}_{AO}}{C_{AB}}, \frac{d\bar{v}_O}{dt} = \frac{\bar{i}_{AO}}{C_O} - \frac{\bar{v}_O}{RC_O} \end{aligned} \quad (6)$$

The duty-ratio constraint consists of replacing the duty cycle  $d_2$  by an expression depending on other variables of the circuit. In Sun et al. (2001), the authors propose to achieve such an expression from the average value of the inductor current waveform, by calculating the peak current directly from the topology equations. To obtain the equation for the duty-ratio constraint in the AIDB, it must be taken into account that  $i_B$  and  $i_{AO}$  have three intervals, therefore it is possible to define  $d_2$  for both currents:

$$d_2 = \frac{2L_B \bar{i}_B}{d_1 T v_g} - d_1 \quad \text{for } i_B \quad (7)$$

$$d_2 = \frac{2L_{AO} \bar{i}_{AO}}{d_1 T (\bar{v}_O - \bar{v}_{AB})} - d_1 \quad \text{for } i_{AO} \quad (8)$$

Following the method proposed by Sun et al. (2001), the expressions obtained for  $d_2$ , (7) and (8), are introduced in the corrected averaging system (6). However, the resulting equations are not in agreement with the steady-state expressions reported in (Arango et al., 2012): introducing (7) in (6), results in a  $i_B$  predicted value close to zero, which is not true as is demonstrated in (Arango et al., 2012). Moreover, the resulting system has Right Hand Plane (RHP) poles that make the predicted model unstable, which is also not accurate, given that an open loop DC/DC converter is always

stable. Similarly, introducing (8) in (6) generates a mathematical problem:  $i_B$  does not appear in the resulting system, therefore it is not possible to obtain a system solution.

Such mathematical inconsistencies made it evident that the revised averaging modeling method is not applicable to the AIDB. Therefore, it was necessary to develop different approaches to calculate  $d_2$  and to model the AIDB dynamic behavior.

### New approach to calculate $d_2$

From the equations of the AIDB topologies given in (1)-(4) it should be noted that in the first and second topologies  $i_B$  and  $i_{AO}$  have opposite slopes, while in the third topology such currents are equal. In addition, from the electrical scheme of the AIDB converter given in Fig. 1, it was noted that the output current  $i_O$  is the aggregated current of the diode  $D_B$  and inductor  $L_{AO}$ , hence  $i_O = i_{AO} + i_{DB}$ . Such conditions are illustrated in Fig. 3, where the waveforms for the discontinuous currents of the AIDB converters are presented for  $D = 0.5$ . The average value of  $i_B$  was calculated from the upper and shaded triangle area:

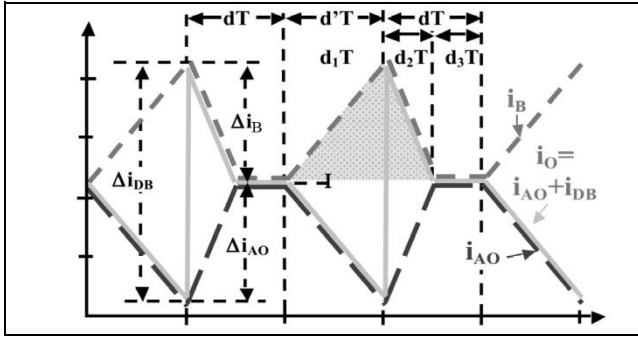


Figure 3. AIDB discontinuous current waveforms

$$\bar{i}_B = \frac{1}{T} \int_0^T i_B dt = I + \frac{\Delta i_B}{2} (d_1 + d_2) \quad (9)$$

Similarly, the average value of  $i_{AO}$  can be calculated from the area of the lower and non-shaded triangle of the same figure:

$$\bar{i}_{AO} = \frac{1}{T} \int_0^T i_{AO} dt = I - \frac{\Delta i_{AO}}{2} (d_1 + d_2) \quad (10)$$

Moreover, the  $L_B$  and  $L_{AO}$  current ripple magnitudes  $\Delta i_B$  and  $\Delta i_{AO}$ , respectively, can be calculated from the first topology equations (2):

$$\Delta i_B = \frac{v_g}{L_B} d_1 T, \Delta i_{AO} = \frac{\bar{v}_O - \bar{v}_{AB}}{L_{AO}} d_1 T \quad (11)$$

Then, the expression for  $d_2$  was obtained by subtracting (10) and (11), and replacing  $\Delta i_B$  and  $\Delta i_{AO}$  with the expressions given in (11). The result is given by:

$$d_2 = 2(\bar{i}_B - \bar{i}_{AO}) / \left( \frac{v_g}{L_B} + \frac{\bar{v}_O - \bar{v}_{AB}}{L_{AO}} \right) d_1 T - d_1 \quad (12)$$

### New averaging approach

As anticipated,  $i_O = i_{AO} + i_{DB}$ , but the revised averaging modeling method of Section 3 does not consider the current in diode  $D_B$ .

Therefore, to obtain a good approximation of the AIDB output current, the diode  $D_B$  current must be included in the analytical model. From the AIDB topologies of Fig. 2, it was noted that diode  $D_B$  conducts in topology 2. Such a topology and its equations were modified to include the current  $i_{DB}$  as given in Fig. 4:

$$\begin{aligned} L_A \frac{di_A}{dt} &= v_g, L_B \frac{di_B}{dt} = v_g - v_O \\ L_{AO} \frac{di_{AO}}{dt} &= v_{AB} \cdot C_{AB} \frac{dv_{AB}}{dt} = -i_{AO} \\ C_O \frac{dv_O}{dt} &= i_{AO} + i_{DB} - \frac{v_O}{R} \end{aligned} \quad (13)$$

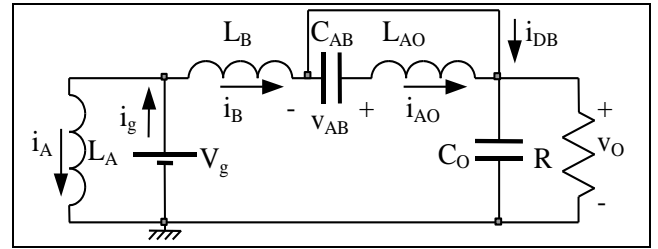


Figure 4. Modified Topology 2. Interval 2:  $d_2$

Therefore, the new state space averaged system for the AIDB is the following:

$$\begin{aligned} \frac{d\bar{i}_A}{dt} &= \frac{v_g - \bar{v}_{AB} d_1}{L_A} \\ \frac{d\bar{i}_B}{dt} &= \frac{v_g}{L_B} (d_1 + d_2) - \frac{\bar{v}_O}{L_B} d_2 + \frac{v_g - \bar{v}_O + \bar{v}_{AB}}{L_B + L_{AO}} d_3 \\ \frac{d\bar{i}_{AO}}{dt} &= \frac{\bar{v}_{AB}}{L_{AO}} (d_1 + d_2) - \frac{\bar{v}_O}{L_{AO}} d_1 + \frac{v_g - \bar{v}_O + \bar{v}_{AB}}{L_B + L_{AO}} d_3 \\ \frac{d\bar{v}_{AB}}{dt} &= \frac{\bar{i}_A d_1 - \bar{i}_{AO}}{C_{AB}} \\ \frac{d\bar{v}_O}{dt} &= \frac{\bar{i}_{AO} + \bar{i}_{DB}}{C_O} - \frac{\bar{v}_O}{RC_O} \end{aligned} \quad (14)$$

where  $d_2$  and  $d_3$  were calculated in (12) and (1), respectively. The new variable  $\bar{i}_{DB}$  represents the average current across the diode  $D_B$ , which only conducts current in the topology 2 as previously described. From Fig. 4 it was noted that  $i_{DB} = i_O - i_{AO}$ , but in such second topology  $i_O = i_B$  as depicted in Fig. 3, therefore  $i_{DB} = i_B - i_{AO}$ .  $\bar{i}_{DB}$  was calculated as given in (15), where the integral of  $i_B$  and  $i_{AO}$  can be calculated by means of triangle areas as depicted in Fig. 3. The peak currents of  $i_B$  and  $i_{AO}$  were calculated from the current slopes in the first topology, obtaining the  $\bar{i}_{DB}$  expression given in (16).

$$\bar{i}_{DB} = \frac{1}{T} \int_{d_1 T}^{(d_1+d_2)T} (i_B - i_{AO}) dt \quad (15)$$

$$\bar{i}_{DB} = \left( \frac{v_g}{L_B} + \frac{\bar{v}_O - \bar{v}_{AB}}{L_{AO}} \right) \frac{d_1 \cdot d_2 \cdot T}{2} \quad (16)$$

and replacing the expression of  $d_2$  given in (12):

$$\bar{i}_{DB} = \left( \frac{v_g}{L_B} + \frac{\bar{v}_O - \bar{v}_{AB}}{L_{AO}} \right) \frac{d_1 T}{2} \left[ \frac{2(\bar{i}_B - \bar{i}_{AO})}{\left( \frac{v_g}{L_B} + \frac{\bar{v}_O - \bar{v}_{AB}}{L_{AO}} \right) d_1 T} - d_1 \right] \quad (17)$$

Then, replacing (1), (12) and (17) in (14), the state space averaged system in terms of the duty cycle  $d_1$  was obtained (18)-(19), where  $d_1 = d' = (1-d)$ . The steady-state condition of the AIDB converter was obtained by solving the system (18)-(19) for the derivatives equal to zero as shown in (20):

$$\begin{aligned} \frac{d\bar{i}_A}{dt} &= \frac{v_g - \bar{v}_{AB}d_1}{L_A} \\ \frac{d\bar{i}_B}{dt} &= \frac{2\bar{i}_B L_B L_{AO}^2(a_1) + 2\bar{i}_{AO} L_B L_{AO}^2(a_2) + \bar{v}_{AB} d_1 T L_B^2(a_3)}{(-V_g L_{AO} - L_B \bar{v}_O + L_B v_{AB}) L_B (L_{AO} + L_B) d_1 T} \\ &\quad + \frac{\bar{v}_O d_1 T L_B L_{AO}(a_4) + d_1 T V_g(a_5)}{(-V_g L_{AO} - L_B \bar{v}_O + L_B v_{AB}) L_B (L_{AO} + L_B) d_1 T} \\ \frac{d\bar{i}_{AO}}{dt} &= \frac{2(\bar{i}_{AO} - \bar{i}_B) L_B L_{AO}(a_6) + d_1 T V_g L_{AO}^2(a_7)}{(-V_g L_{AO} - L_B \bar{v}_O + L_B v_{AB}) L_{AO} (L_{AO} + L_B) d_1 T} \\ &\quad + \frac{\bar{v}_O d_1^2 T L_B(a_8) + d_1 T L_{AO} L_B(a_9)}{(-V_g L_{AO} - L_B \bar{v}_O + L_B v_{AB}) L_{AO} (L_{AO} + L_B) d_1 T} \\ \frac{d\bar{v}_{AB}}{dt} &= \frac{\bar{i}_A d_1 - \bar{i}_{AO}}{C_{AB}} \\ \frac{d\bar{v}_O}{dt} &= \frac{R_L [2\bar{i}_B L_B L_{AO} - d_1^2 T (V_g L_{AO} + \bar{v}_O L_B - \bar{v}_{AB} L_B)]}{C_O R_L L_B L_{AO}} \\ &\quad - \frac{2\bar{v}_O L_B L_{AO}}{C_O R_L L_B L_{AO}} \end{aligned} \quad (18)$$

$$\begin{aligned} a_1 &= -V_g + \bar{v}_O + \bar{v}_{AB}, \quad a_2 = V_g - \bar{v}_O - \bar{v}_{AB}, \\ a_3 &= V_g + \bar{v}_{AB} + \bar{v}_O d_1 - 2\bar{v}_O, \quad a_4 = V_g - d_1 V_g + d_1 \bar{v}_{AB} - d_1 \bar{v}_O \\ a_5 &= (-V_g - \bar{v}_{AB}) L_B L_{AO} - \bar{v}_O L_B^2 - \bar{v}_O d_1 L_{AO}^2, \\ a_6 &= (-V_g + \bar{v}_O) L_{AO} + \bar{v}_{AB} L_B, \quad a_7 = -V_g + \bar{v}_O (d_1 + 1) - \bar{v}_{AB}, \\ a_8 &= -\bar{v}_{AB} + \bar{v}_O, \\ a_9 &= d_1 \bar{v}_O (V_g - \bar{v}_{AB}) + V_g (\bar{v}_{AB} - \bar{v}_O) - 2\bar{v}_{AB} \bar{v}_O + \bar{v}_{AB}^2 + \bar{v}_O^2 \end{aligned} \quad (19)$$

Such expressions allow us to design the AIDB converter for a given application's requirements following the procedure proposed in (Arango et al., 2012). Then, the state space averaged system of (18)-(19) can be linearized around the operating point (20) in the following form of (21):

$$\begin{aligned} I_A &= \frac{1}{D'} \left( 1 + \frac{1}{D'} \right) \frac{V_g}{R} - \frac{V_g}{2} \left( \frac{L_B + L_{AO}}{L_B L_{AO}} \right) D'^2 T \\ I_B &= \left( 1 + \frac{1}{D'} \right) \frac{V_g}{R} + \frac{V_g}{2} \left( \frac{L_B + L_{AO}}{L_B L_{AO}} \right) D'^2 T \\ I_{AO} &= \left( 1 + \frac{1}{D'} \right) \frac{V_g}{R} - \frac{V_g}{2} \left( \frac{L_B + L_{AO}}{L_B L_{AO}} \right) D'^3 T \\ V_{AB} &= \frac{V_g}{D'}, \quad V_O = \left( 1 + \frac{1}{D'} \right) V_g \end{aligned} \quad (20)$$

$$\hat{\dot{x}} = A \hat{x} + B \hat{d}_1 \quad (21)$$

where A is the Jacobian matrix of (18) regarding to the state variables  $\hat{x}$  (22) and B is the Jacobian matrix of (18) regarding to the duty cycle  $d_1$ . Both Jacobian Matrices were evaluated at the operating point, as is shown in (23), where f represents each one of the functions of (18) used to calculate  $\hat{x}$ .

$$\hat{x} = [\hat{i}_A \quad \hat{i}_B \quad \hat{i}_{AO} \quad \hat{v}_{AB} \quad \hat{v}_O]^T \quad (22)$$

$$A = \left. \frac{\partial f(\bar{x}, d_1)}{\partial \bar{x}} \right|_{\bar{x}=X, d_1=D'}, \quad B = \left. \frac{\partial f(\bar{x}, d_1)}{\partial d_1} \right|_{\bar{x}=X, d_1=D'} \quad (23)$$

## Model validation

The proposed model was validated by contrasting its behavior with the time and frequency responses of the AIDB circuit implemented in the electrical simulator PSIM, which is a standard for power electronics applications.

The AIDB parameters used for the validation were extracted from the photovoltaic application described in (Arango et al., 2012), where the steady-state input and output voltages are  $V_g = 10$  V and  $V_O = 30$  V, respectively, it requiring a duty cycle,  $D = 0.5$ . In addition, the application adopts  $L_A = L_B = L_{AO} = 200$   $\mu$ H,  $C_{AB} = 50$   $\mu$ F,  $C_O = 20.83$   $\mu$ F, a load impedance  $R = 10$   $\Omega$  and a switching frequency of  $f_{sw} = 50$  kHz ( $T = 20$   $\mu$ s).

In this system, once matrices A and B are obtained, and before the numeric values are replaced, it becomes necessary to make a time-normalization to avoid numerical errors caused by the large difference between the magnitudes of some components of the matrices. This normalization consists of a change in the time scale and passive elements magnitude (Arango, Calvente, Giral, Aroudi, and Martinez-Salamero, 2005):

$$\begin{aligned} t_N &= t / 10^{-6}, \quad C_{AB,N} = C_{AB} / 10^{-6}, \quad C_{O,N} = C_O / 10^{-6} \\ L_{A,N} &= L_A / 10^{-6}, \quad L_{B,N} = L_B / 10^{-6}, \quad L_{AO,N} = L_{AO} / 10^{-6} \end{aligned} \quad (24)$$

where  $t_N$  represents the normalized time variable, while  $C_{i,N}$  and  $L_{i,N}$  are the normalized passive elements. The non-normalized parameters were used to calculate the steady-state operating point given in (25), and the normalized parameters were used to calculate the A and B matrixes (26).

$$\begin{aligned} I_A &= 5.752 \text{ A}, \quad I_B = 3.25 \text{ A}, \quad I_{AO} = 2.876 \text{ A}, \\ V_{AB} &= 20 \text{ V}, \quad V_O = 30 \text{ V} \end{aligned} \quad (25)$$

$$A = \begin{bmatrix} 0 & 0 & 0 & -0.0025 & 0 \\ 0 & -0.2 & 0.2 & -0.003114 & 0.001875 \\ 0 & 0.2 & -0.2 & 0.00812 & -0.00688 \\ 0.01 & 0 & -0.02 & 0 & 0 \\ 0 & 0.4255 & 0 & 0.000532 & -0.004788 \end{bmatrix} \quad (26)$$

$$B = [-0.1 \quad 0.2998 \quad -0.3 \quad 0.115 \quad -0.04255]^T$$

The expression in (27) shows the control-to-output transfer function, in which the normalization was removed, to contrast the model behavior with a circuital simulation. As expected, the transfer function is a fifth order one, and all the system poles are at the

left half-plane, which ensures the stability of the open-loop AIDB converter.

$$G(s) = \frac{\hat{v}_o(s)}{\hat{d}(s)} = \frac{-42550(s + 7.67 \cdot 10^4)}{(s^2 + 1785s + 1.65 \cdot 10^7)} \cdot \frac{(s^2 - 2.58 \cdot 10^4)(s - 8895)(s + 5.67 \cdot 10^4)}{(s^2 + 2812s + 1.61 \cdot 10^8)(s + 4 \cdot 10^5)} \quad (27)$$

The first test was performed in time-domain: the mathematical model, implemented in Matlab and the circuital scheme, implemented in PSIM, were simulated for a 1 % perturbation on  $d_1$ . Fig. 5 shows the dynamic responses of both model and circuital simulation, where the agreement between plots is evident. It was noted that the mathematical model does not reproduce the voltage ripple exhibited by the non-linear circuital, which was expected since the proposed model is based on the differential equations averaged in the switching period.

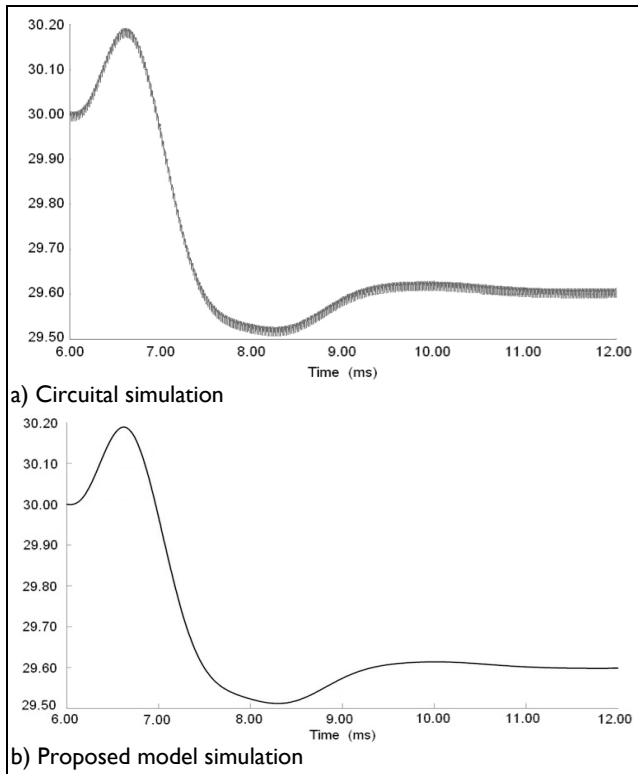


Figure 5. Proposed model validation in time domain: output voltage [V] response to 1% change in  $d_1$

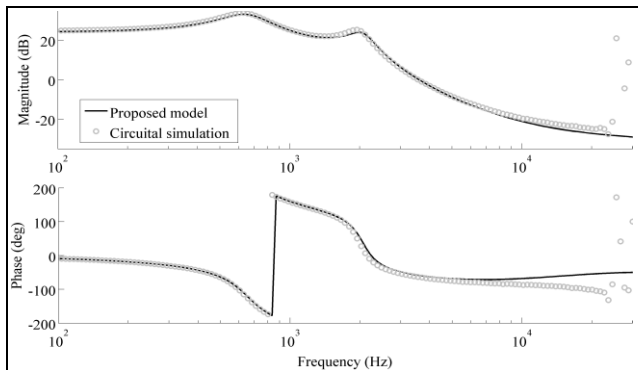


Figure 6. Proposed model validation in frequency domain: bode diagrams

The second test was performed in frequency-domain: the bode diagram of both the proposed model and circuital scheme were calculated between 100 Hz and 25 kHz, the latter constrained by the Nyquist frequency in which the linear approximation is no longer valid. Fig. 6 shows the frequency responses of both model and circuit, where the model performs a satisfactory reproduction of the non-linear circuit up to 20 kHz. An increased error in both magnitude and phase was observed for frequencies larger than 10 kHz, this was caused by the voltage ripple frequency components.

Both time and frequency tests evidenced the accurate approximation of the non-linear circuit dynamics provided by the proposed model.

### Application example

To illustrate the usefulness of the proposed model in control-oriented applications, a Linear-Quadratic Regulator (LQR) (Ogata, 2009), was designed to control the AIDB converter. The LQR scheme was used to control systems by choosing a control vector  $u(t)$  such that a given performance index is minimized. Therefore, the design problem is reduced to determining the matrix  $K$  in (28) that minimizes the index  $J$ , where  $Q$  is a positive-definite (or positive-semidefinite) Hermitian or real symmetric matrix and  $R$  is a positive-definite Hermitian or real symmetric matrix. The matrices  $Q$  and  $R$  determine the relative importance of the error and the distribution of the energy in the system states. The detailed derivation of matrix  $K$  is presented by Ogata (2009).

$$u(t) = -Kx(t), \quad J = u^* \int_0^{\infty} (x^* Q x + u^* R u) dt \quad (28)$$

The matrices  $Q$  and  $R$  are usually selected by the designer, using knowledge about the system (Ogata, 2009). To regulate the AIDB converter, the matrices  $Q$  and  $R$  were defined from energy considerations and from the relative weight of the output voltage and the error. The error to the reference  $V_{ref} = 30$  V, was introduced in the controller design with an additional averaged state  $\bar{e}$  (29). Then, the coefficients in (30) were defined.

$$\frac{d\bar{e}}{dt} = \bar{v}_O - V_{ref} \quad (29)$$

$$\begin{bmatrix} QI_A = (5.95)^2 \times 1 \\ QI_B = (3.05)^2 \times 1 \\ QI_{AO} = (2.97)^2 \times 1 \\ QV_{AB} = (20)^2 \times 50 \times 10^{-3} \\ QV_O = (30)^2 \times 20 \\ QE = 1 \times 10^{10} \end{bmatrix} \quad (30)$$

Such coefficients were used to give a higher weight to the variables of major interest: the output voltage and the error. The final matrices  $Q$  and  $R$  are:

$$Q = \frac{1}{QV_O} \begin{bmatrix} QI_A & 0 & 0 & 0 & 0 & 0 \\ 0 & QI_B & 0 & 0 & 0 & 0 \\ 0 & 0 & QI_{AO} & 0 & 0 & 0 \\ 0 & 0 & 0 & QV_{AB} & 0 & 0 \\ 0 & 0 & 0 & 0 & QV_O & 0 \\ 0 & 0 & 0 & 0 & 0 & QE \end{bmatrix} \quad (31)$$

$$R = [1]$$

where matrix R is small enough to perform a fast correction of the perturbations. Then, using the Matlab command  $\text{lqr}(A,B,Q,R)$ , matrix K was calculated:

$$K = [-3.79 \quad 0.12 \quad 0.10 \quad -0.40 \quad 0.31 \quad -745] \quad (32)$$

Such LQR strategy, implemented with K in (32), was tested with both a mathematical model (in Matlab) and a non-linear circuit (in PSIM). Fig. 7 reports the simulation results: in both cases the LQR achieves null steady state error, even considering a 10 % perturbation on dI. Moreover, both responses are in agreement, which reinforces the model accuracy. Finally, the satisfactory circuital response shows the usefulness of the proposed model in control design applications.

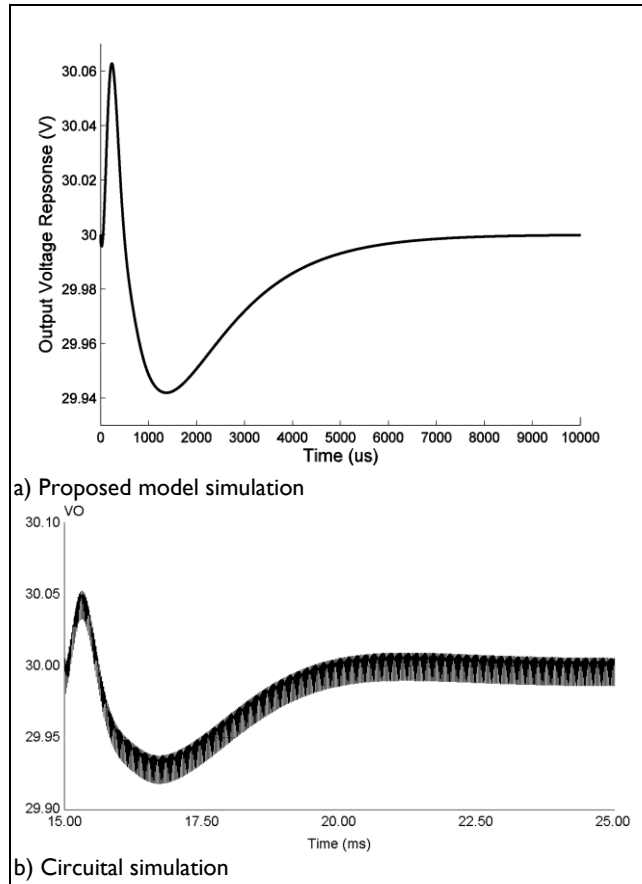


Figure 7. Closed loop AIDB with K in (32)

## Conclusions

Classical CCM and revised averaging modeling methods are not suitable for the AIDB converter due to its special characteristics.

Therefore, a new approach was developed starting from the revised averaging, but considering a diode current that is typically disregarded. Moreover, a novel correction to the second duty cycle was developed to obtain a new state space averaged system, which accurately describes the AIDB dynamic performance.

## Acknowledgements

This work was supported by GAUNAL group of the Universidad Nacional de Colombia under the projects SMART-ALEN and VECTORIAL-MPPT and by COLCIENCIAS under the doctoral scholarship 095-2005.

## References

- Ahmed, N. A., Miyatake, M., Al-Othman, A. K., Power fluctuations suppression of stand-alone hybrid generation combining solar photovoltaic/wind turbine and fuel cell systems., *Energy Conversion and Management*, Vol. 49, Oct., 2008, pp. 2711-2719.
- Arango, E., Calvente, J., Giral, R., Aroudi, A. E., Martinez-Salamero, L., LQR control of an asymmetrical interleaved boost converter working in inherent DCM., *Proceedings of the IEEE ISIE Conference*, Dubrovnik, June, 2005, pp. 721-726.
- Arango, E., Ramos-Paja, C. A., Saavedra-Montes, A. J., Design of asymmetrical boost converters based on photovoltaic systems requirements., *Dyna*, Vol. 79, Jan., 2012, pp. 31-40.
- Erickson, R. W., Maksimovic, D., *Fundamentals of power electronics*, Springer (Ed.), New York, Chapman & Hall, 2001.
- Giral, R., Martinez-Salamero, L., Singer, S., Interleaved converters operation based on CMC., *IEEE Transactions on Power Electronics*, Vol. 14, Jul., 1999, pp. 643-652.
- Jain, S., Agarwal, V., New current control based MPPT technique for single stage grid connected PV systems., *Energy Conversion and Management*, Vol. 48, Feb., 2007, pp. 625-644.
- Ilango, G. S., Rajasekar, N., An improved energy saving v/f control technique for solar powered single-phase induction motor., *Energy Conversion and Management*, Vol. 50, Dec., 2009, pp. 2913-2918.
- Ogata K., *Modern Control Engineering*, 5th Ed., Prentice Hall, 2009.
- Ouyang, W., Cheng, H., Zhang, X., Yao, L., Distribution network planning method considering distributed generation for peak cutting., *Energy Conversion and Management*, Vol. 51, Dec., 2010, pp. 2394-2401.
- Prudente, M., Pfitscher, L. L., Emmendoerfer, L. L., Romaneli, E. F., Gules, E. F., Voltage Multiplier Cells Applied to Non-Isolated DC-DC Converters., *IEEE Transactions on Power Electronics*, Vol. 23, Mar., 2008, pp. 871-887.
- Sun, J., Mitchell, D. M., Greuel, M. F., Krein, P. T., Bass, R. M., Averaged modeling of PWM converters operating in discontinuous conduction mode., *IEEE Transactions on Power Electronics*, Vol. 16, Jul., 2001, pp. 482-492.
- Veerachary, M., Senjyu, T., Uezato, K., Maximum power point tracking control of IDB converter supplied PV system., *IEE Proceedings - Electric Power Applications*, Vol. 148, Nov., 2001, pp. 494-502.